doi.org/10.36721/PJPS.2026.39.11.309.1

Mechanisms of Quyu tong-bi decoction for the treatment of type III prostatitis - based on database and *in-vitro* experiments

Miaomiao Ma[1,2#], Zulong Wang[1#] and Baojun Ju[1*]

[1]Department of Andrology, The First Affiliated Hospital of Henan University of Chinese Medicine, Zhengzhou, China
[2]The First Clinical Medical College of Henan University of Chinese Medicine, Zhengzhou, China

Abstract: **Background**: Quyu tong-bi decoction (QYTB) has demonstrated significant clinical efficacy in treating type III prostatitis. However, its underlying pharmacological mechanisms remain to be fully elucidated. **Objectives**: This study aimed to investigate the molecular mechanisms by which QYTB addresses type III prostatitis by integrating network pharmacology, molecular docking and experimental validation. **Methods**: Active ingredients and potential targets of QYTB were retrieved from the TCMSP and UniProt databases. Disease-associated targets for type III prostatitis were collected from GeneCards, OMIM and TTD. After identifying drug-disease intersection targets, protein-protein interaction (PPI) networks and topological analyses were performed using Cytoscape and STRING. GO and KEGG enrichment analyses were conducted via Metascape. Finally, molecular docking and *in-vitro* experiments using SP-induced rat spinal cord astrocytes were performed for validation. **Results**: Thirty-two core targets of QYTB were identified, primarily involving oxidative stress, inflammatory response and apoptosis. *In-vitro* validation revealed that QYTB-containing serum notably upregulated the concentrations of CAT, SOD and GSH in SP-induced astrocytes while reducing MDA levels. Furthermore, QYTB downregulated pro-inflammatory markers (IL-6, TNF-α and IL-1β) and suppressed the phosphorylation of p38MAPK and CREB within the MAPK signaling pathway. **Conclusion**: QYTB exerts potent antioxidant and anti-inflammatory effects in the treatment of type III prostatitis, likely through the modulation of the MAPK signaling pathway.

Keywords: Chronic prostatitis; Inflammation; MAPK signaling pathway; Network pharmacology; Oxidative stress

Submitted on 08-11-2025 – Revised on 12-03-2026 – Accepted on 18-03-2026

INTRODUCTION

Type III prostatitis is a prevalent clinical condition in andrology and urology, primarily characterized by persistent pelvic pain and urinary abnormalities, with a reported incidence ranging from 6.0% to 32.9% (Ma *et al*., 2025). Modern lifestyle factors, such as prolonged sitting and physical inactivity, are increasingly recognized as contributing to the onset and progression of the disease, which significantly impairs the quality of life and mental well-being of patients. Despite its high prevalence, the exact pathogenesis of type III prostatitis remains to be fully elucidated. Recent evidence suggests that the refractory pelvic pain associated with this condition is not merely a localized inflammatory event but involves central sensitization (Jiang *et al*., 2024). In this process, peripheral inflammatory mediators-particularly Substance P (SP)-transmit noxious stimuli to the spinal cord, triggering the pathological activation of spinal cord astrocytes. These activated astrocytes subsequently release neuro-inflammatory cytokines, establishing a self-perpetuating cycle of chronic pain (Nurnberger *et al*., 2023).

Current clinical management often focuses on symptom relief and quality-of-life improvement, frequently employing a combination of α-receptor blockers, antibiotics and non-steroidal anti-inflammatory drugs (Valipour *et al*., 2025). However, many of these are empirical treatments that lack robust evidence-based support, often resulting in poor long-term efficacy (Zbiciak-Nylec *et al*., 2021). Conventional therapies, such as antibiotics (e.g., levofloxacin) and α-blockers, typically yield suboptimal outcomes because they primarily target single pathways. In contrast, Quyu tong-bi decoction (QYTB), a classical Chinese herbal formula, offers a multi-component and multi-target therapeutic advantage. Previous clinical practice by the research team has demonstrated that QYTB effectively improves hemorheology and the expression of inflammatory mediators in patients with type III prostatitis. Distinct from earlier research focusing solely on peripheral anti-inflammation, this study explores for the first time how QYTB disrupts the pathological crosstalk between neuroinflammation and oxidative stress by modulating the MAPK pathway in spinal astrocytes.

In the present study, the authors utilized network pharmacology and molecular docking to predict the active ingredients of QYTB, identify therapeutic targets and evaluate the binding affinities between compounds and anticipated proteins. For experimental validation, an *in-vitro* model was established using SP-induced rat spinal cord astrocytes to simulate the neuroinflammatory microenvironment of type III prostatitis. Levofloxacin was selected as the positive control, since it is widely

*Corresponding author: e-mail: jubaojun@hactcm.edu.cn
#These authors contributed equally and are the co-first authors.

recommended in clinical guidelines as a primary empirical treatment (Qin *et al*., 2022). Although predominantly an antibiotic, levofloxacin has demonstrated potential anti-inflammatory and immunomodulatory properties that contribute to symptom relief in chronic pelvic pain syndrome (Borgert *et al*., 2025). By integrating computational predictions with experimental techniques-including CCK-8, ELISA and Western blot-this study aims to investigate the underlying mechanisms of QYTB, providing a foundational scientific resource for the application of traditional Chinese medicine in the therapeutic intervention of type III prostatitis.

MATERIALS AND METHODS

The databases utilized in this study were accessed on November 19, 2024, to ensure the temporal relevance and reproducibility of the data.

Active compounds and corresponding targets

The chemical components of QYTB—comprising *Cistanche deserticola, Rehmannia glutinosa, Schisandra chinensis, Cuscuta chinensis, Prunus persica, Carthamus tinctorius, Ligusticum chuanxiong, Alisma orientale, Tetrapanax papyriferus, Achyranthes bidentata, Plantago asiatica, Dianthus superbus, Evodia rutaecarpa and Psoralea corylifolia*—were retrieved from the Traditional Chinese Medicine Systems Pharmacology (TCMSP) database. Potential active ingredients were screened based on a minimum oral bioavailability (OB) of 30% and a drug-likeness (DL) index of ≥ 0.18. The target proteins associated with these active ingredients were subsequently converted into human gene symbols using the UniProt database.

Disease targets

Disease-associated targets for type III prostatitis were identified by searching the GeneCards (https://www.genecards.org/), OMIM (http://omim.org/) and TTD (http://db.idrblab.net/ttd/) databases. The search keywords included "type III prostatitis", "CP/CPPS", "Chronic prostatitis" and "Chronic non-bacterial prostatitis". After deduplication, Gene Cards relevance score cut-offs ≥ 20% was applied to ensure the selection of high-confidence disease targets.

Screening of drug-disease intersection targets

The intersection of drug-related and disease-associated targets was determined using Venny 2.1 and the overlapping genes were visualized through a Venn diagram.

Screening and visualization of core components

The interactions between active ingredients and their corresponding targets were illustrated using Cytoscape (version 3.9.1) to construct a component-target network. Topological analysis was performed via the Cytoscape-NCA plugin to identify the core active components of QYTB for the treatment of type III prostatitis.

Screening and visualization of core targets

The intersecting targets were analyzed using STRING 11.5 to construct a protein-protein interaction (PPI) network, which was subsequently visualized in Cytoscape 3.9.1. Topological analysis was conducted using the CytoscapeNCA plugin. Furthermore, the MCODE plugin was employed to extract central subnetworks and identify the primary therapeutic targets of QYTB.

GO and KEGG analysis

The Metascape database was utilized for Gene Ontology (GO) and Kyoto Encyclopedia of Genes and Genomes (KEGG) enrichment analyses of the intersection targets. The analysis followed standard criteria: a significance threshold of $P < 0.01$, a minimum gene count of 3 and an enrichment factor > 1.5. Visualization of the enrichment results was performed using the Microbioinformatics platform (www.bioinformatics.com.cn/).

Construction of drug-ingredient-target network

A core network representing the multi-component and multi-target mechanisms of QYTB in treating type III prostatitis was constructed by integrating the ingredients of the fourteen constituent herbs with the intersection targets. The network was visualized using Cytoscape 3.9.1.

Molecular docking

The molecular configurations of the candidate compounds were sourced from the PubChem database (https://pubchem.ncbi.nlm.nih.gov) and optimized through energy minimization using Chem3D. Three-dimensional protein structures were retrieved from the PDB database. PyMOL software was utilized for the removal of water molecules and original ligands from the protein structures.

Molecular docking was performed with the proteins as receptors and the active compounds as ligands. AutoDockTools (version 1.5.7) was used to add hydrogen atoms and calculate partial charges for the receptors, while format conversion was performed for the small molecules. The binding affinities between ligands and receptors were calculated using AutoDock Vina. The resulting docking complexes with the highest affinities were visualized in PyMOL to analyze hydrogen bond interactions, calculate bond distances and display the molecular stick structures within the surface active pockets.

Experimental verification

Reagents

The following reagents and kits were used in this study: Rat spinal cord astrocyte complete culture medium (Puno, CM-R306); Penicillin-Streptomycin mixed solution (100X) (Solarbio, P1400); Trypsin-EDTA digestion solution (Solarbio, T1320); Substance (Shanghai Taoshu, TP1087); CCK-8 (Solarbio, CA1210); Total superoxide dismutase (SOD) assay kit (Nanjing Jiancheng, A001-3-1); Glutathione peroxidase (G58-FI) assay kit (Nanjing

Jiancheng, A005-1-2); Catalase (CAT) assay kit (Nanjing Jiancheng, A007-1-1); Malondialdehyde (MDA) assay kit (Nanjing Jiancheng, A003-1-1); RIPA (EpiZyme, PC101); BCA protein quantification kit (EpiZyme, ZJ101); TNF-α antibody (Affinity, AF7014); IL-6 antibody (Affinity, A20798); IL-1β antibody (abcam, ab254360); p38 alpha/MAPK14 antibody (abcam, ab170099); p-p38 MAPK antibody (Bioss, bs-5476R); CREB antibody (Bioss, bs-0035R); p-CREB antibody (Bioss, bs-0036R); GAPDH antibody (abcam, ab181602); Rabbit anti-GAPDH (Bioworld, AP0063); Goat anti-rabbit IgG (Earth Biology, E030120-01).

Preparation of drug-containing serum

The QYTB formula consisted of *Cistanche deserticola* (25g), *Rehmannia glutinosa* (20g), *Schisandra chinensis* (12g), *Cuscuta chinensis* (12g), *Prunus persica* (12g), *Carthamus tinctorius* (12g), *Ligusticum chuanxiong* (12g), *Alisma orientale* (15g), *Tetrapanax papyriferus* (6g), *Achyranthes bidentata* (15g), *Plantago asiatica* (15g), *Dianthus superbus* (15g), *Evodia rutaecarpa* (3g) and *Psoralea corylifolia* (10g). The herbs were provided by the Chinese Medicine Pharmacy of the First Affiliated Hospital of Henan University of Chinese Medicine. The mixture was soaked in 2000 mL of water for 30 minutes, boiled for 30 minutes and filtered. The residue was boiled again in 2000 mL of water for 30 minutes and filtered. The two filtrates were combined and concentrated to 2 g/mL using a rotary evaporator, then stored at 4°C. Levofloxacin tablets (Guangdong Dongyangguang Pharmaceutical Co., Ltd., National Drug Approval No. H20183513, specification 0.25g×12s) were ground into powder and dissolved in distilled water to prepare a 2.5 mg/mL suspension.

Thirty male Sprague-Dawley (SD) rats (8 weeks old, weighing 270 ± 20 g; Animal License No. SCXK (Beijing) 2019-0008) were obtained from Beijing Huafukang Biotechnology Co., Ltd. The rats were housed in a temperature-controlled room (22 ± 2°C) with a 12 h light/dark cycle and standard humidity (50%–60%), with free access to standard rodent chow and water. After five days of adaptive feeding, the rats were randomly assigned to three groups (n = 10 per group) using a computer-generated random number table: control, QYTB and levofloxacin. Cages from different groups were distributed systematically on the racks. The control group received 1 mL/100g physiological saline, the QYTB group received 33 mg/kg QYTB solution and the levofloxacin group received 22.5 mg/kg levofloxacin suspension via gavage once daily for seven days. Two hours after the final administration, blood was collected from the abdominal aorta under anesthesia. Serum was separated by centrifugation, sterilized using a 0.2 μm filter and stored at -80°C.

Cell culture

Rat spinal cord astrocytes (Puno, CP-R306) were cultured in complete medium at 37°C with 5% CO_2. Upon reaching 80% confluence, cells were digested with trypsin and passaged. Third-generation cells were used for all subsequent experiments.

CCK-8 screening of optimal drug-containing serum concentration

Cells were seeded in 96-well plates at a density of 8×10^3 cells/well. At 80% confluence, cells were incubated with varying concentrations of QYTB-containing serum, levofloxacin-containing serum, or normal rat serum (control) for 12 hours. CCK-8 solution was added and incubated for 2 hours. Cell viability was determined by measuring optical density (OD) at 450 nm using a microplate reader to identify the optimal intervention concentration.

Experimental grouping and intervention measures

Cells were assigned to four groups: (1) Control (normal rat serum); (2) Model (SP + normal rat serum); (3) QYTB (SP + optimal concentration of QYTB serum); and (4) Levofloxacin (SP + optimal concentration of levofloxacin serum).

Enzyme-linked immunosorbent assay

The levels of biochemical markers were measured using ELISA kits according to the manufacturer's instructions.

Western blot

Cells were lysed on ice using RIPA buffer and protein concentrations were determined with a BCA kit. Protein samples were separated via SDS-PAGE and transferred onto membranes. Membranes were blocked with 5% TBST-skimmed milk for 2 hours, washed with TBST and incubated with primary antibodies. Following three washes, membranes were incubated with secondary antibodies (1:10,000) at room temperature for 2 hours. Protein bands were developed using enhanced chemiluminescence (ECL).

Statistical analysis

Data were analyzed using GraphPad Prism 9.5.0 and expressed as the mean ± standard deviation ($\bar{x} \pm s$) Differences between groups were assessed via one-way ANOVA followed by Dunnett's multiple comparison test. $P < 0.05$ was considered statistically significant.

RESULTS

Active ingredients and targets of drugs

The initial screening yielded varying numbers of active ingredients for each constituent herb: 6 for Roucongrong (Cistanche deserticola), 2 for Shudihuang (*Rehmannia glutinosa*), 21 for Wuweizi (*Schisandra chinensis*), 11 for Tusizi (*Cuscuta chinensis*), 23 for Taoren (*Prunus persica*), 22 for Honghua (*Carthamus tinctorius*), 4 for Lulutong (*Liquidambar formosana*), 10 for Zexie (*Alisma orientale*), 4 for Tongcao (*Tetrapanax papyriferus*), 20 for Niuxi

(*Achyranthes bidentata*), 6 for Bianxu (*Polygonum aviculare*), 6 for Qumai (*Dianthus superbus*), 30 for Wuzhuyu (*Evodia rutaecarpa*) and 2 for Buguzhi (*Psoralea corylifolia*). After the removal of redundant entries, a total of 139 unique active ingredients associated with QYTB were identified.

Subsequently, the target proteins of these drugs were converted into human gene symbols via the UniProt database. The number of drug targets for each herb was as follows: 175 for Roucongrong, 31 for Shudihuang, 21 for Wuweizi, 213 for Tusizi, 52 for Taoren, 216 for Honghua, 55 for Lulutong, 5 for Zexie, 3 for Tongcao, 211 for Niuxi, 178 for Bianxu, 43 for Qumai, 166 for Wuzhuyu and 29 for Buguzhi. After deduplication, 276 unique potential targets for QYTB were obtained.

Disease target screening

Disease targets were identified by searching the GeneCards, OMIM and TTD databases using relevant keywords. Following the merging and deduplication of results from these three sources, a total of 6,541 potential disease targets were collected. By applying a relevance score threshold of ≥ 20 in GeneCards, 520 highly relevant targets for type III prostatitis were ultimately selected for further analysis.

Screening of drug-disease intersection targets

The intersection of the 276 QYTB-related targets and the 520 highly relevant disease targets yielded 119 overlapping genes, which are visualized in the Venn diagram shown in Fig. 1.

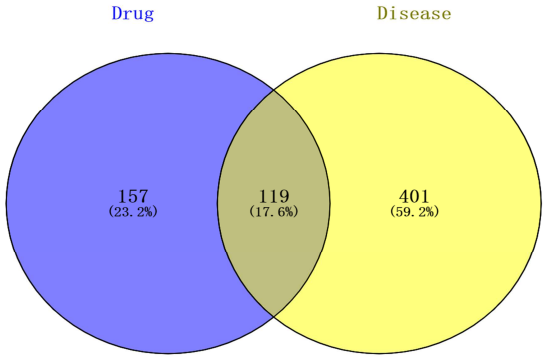

Fig. 1: Drug-disease intersection targets
Drug: QYTB; Disease: type III prostatitis

Screening of core components

Data pertaining to the 139 active components and their 119 intersection targets were integrated into Cytoscape and topological analysis was performed using the CytoscapeNCA plugin. The top-ranked active ingredients included quercetin, kaempferol, beta-sitosterol, stigmasterol and luteolin, which were predicted as the primary therapeutic components of QYTB for treating type III prostatitis. The top 10 drug components are summarized in Table 1. A component-target visualization network was constructed (Fig. 2), in which the node size is proportional to the interaction degree of each component.

Screening and visualization of core targets

A protein-protein interaction (PPI) network was constructed based on the 119 intersection targets using the *"Homo sapiens"* parameter and a minimum interaction confidence score of 0.4. The resulting network comprised 119 nodes and 3,142 edges, which is approximately 3.45 times the expected number of edges (912), indicating strong biological connectivity and interaction potential among the targets. Topological analysis was performed using the CytoscapeNCA plugin to calculate the degree centrality (DC), betweenness centrality (BC) and closeness centrality (CC) for each target. The MCODE plugin was then employed to extract the core subnetwork. Based on the median values of DC, BC and CC, a total of 32 core targets were identified within the central subnetwork (Table 2, Fig. 4).

GO and KEGG analysis

Functional enrichment analyses, including Gene Ontology (GO) and Kyoto Encyclopedia of Genes and Genomes (KEGG), were performed on the intersection targets. The analysis identified a total of 1,758 significant biological processes (BP), 88 cellular components (CC) and 152 molecular functions (MF), alongside 180 enriched pathways. The BP category primarily involved responses to oxidative stress and the regulation of apoptotic processes. The CC category was mainly associated with membrane rafts, membrane microdomains and vesicular lumens. Key MF included kinase binding, cytokine receptor binding and transcription factor binding. The top 10 entries for each GO category are visualized in a bar chart (Fig. 4A).

KEGG analysis revealed that the primary enriched pathways included the PI3K-Akt, IL-17 and MAPK signaling pathways. The top 15 pathways most relevant to the pathogenesis of type III prostatitis were selected to construct a bubble chart (Fig. 4B).

Network diagram for drug-active ingredient-target interactions

The active ingredients of the fourteen constituent herbs—including *Cistanche deserticola, Rehmannia glutinosa* and *Schisandra chinensis*, among others—were integrated with the intersection target data into Cytoscape. This allowed for the visualization of the complex interaction relationships between the drugs, their components and the targets. The resulting core network illustrates the multi-target therapeutic mechanism of QYTB in treating type III prostatitis (Fig. 5).

Table 1: Ranking of QYTB components for the treatment of type III prostatitis

MOL ID	Compound	Degree	Betweenness
MOL000098	quercetin	860	73375.91
MOL000422	kaempferol	248	15932.33
MOL000358	beta-sitosterol	239	16777.56
MOL000449	stigmasterol	115	9876.98
MOL000006	luteolin	114	10121.59
MOL002714	baicalein	74	8202.41
MOL000354	emodin	45	5854.97
MOL000173	sesamin	45	5093.05
MOL000472	palmatine	35	6430.11
MOL001558	gomisin R	23	11297.29

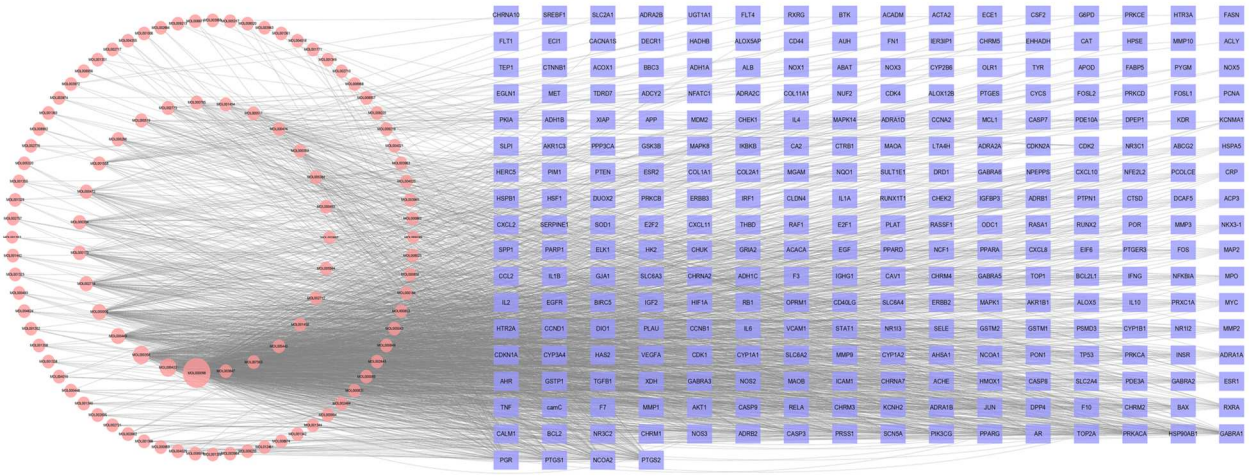

Fig. 2: Component-target network diagram
The pink circle represents the chemical constituents of QYTB, while the purple rectangle represents the disease targets for type III prostatitis.

Molecular docking

Molecular docking was performed to validate the binding affinities between the top 5 core compounds and the primary therapeutic targets. The top 5 compounds were selected due to their high degree centrality in the ingredient-target network, identifying them as the most potent multi-target components of QYTB. The core targets were chosen based on their location within the MCODE-identified central subnetwork and their fulfillment of the screening criteria, marking them as the most critical nodes in the disease-drug interaction. Binding affinities are summarized in Table 3. A negative binding energy indicates that the interaction between the ligand and receptor occurs spontaneously. Generally, a binding energy ≤ -5.0 kcal/mol suggests favorable binding, while an affinity ≤ -7.0 kcal/mol signifies robust binding interaction (Ge *et al*., 2025).

The results showed that 100% of the docking complexes achieved a binding energy ≤ -5.0 kcal/mol and 60% demonstrated affinities ≤ -7.0 kcal/mol. These findings indicate that the core components of QYTB can form stable complexes with their targets, exhibiting possess strong targeting properties. The structural complexes were visualized using PyMOL, displaying the molecular stick structures within the protein surface active pockets. Hydrogen bond distances between ligands and amino acid residues are represented by yellow dashed lines. Representative docking complexes are presented in Fig. 6.

Experimental verification

CCK-8

To further investigate the pharmacological mechanisms of QYTB, levofloxacin was employed as a positive control. Primary rat spinal cord astrocytes were incubated with varying concentrations of serum containing either QYTB or levofloxacin. The results demonstrated that QYTB-containing serum (5–30%) and levofloxacin-containing serum (5–25%) exhibited no adverse effects on astrocyte viability (Fig. 7A Fig. 7B). Furthermore, when these drug-containing sera were incubated with SP-induced astrocytes, cell viability remained comparable to that of the control group ($P > 0.05$), indicating a lack of cytotoxicity within these concentration ranges (Fig. 7C Fig. 7D). To avoid potential interference from the lysis reagent while ensuring therapeutic efficacy, a 5% concentration of both QYTB-containing and levofloxacin-containing serum was selected for all subsequent analyses.

Table 2: Core targets of QYTB in the treatment of type III prostatitis

Name	MCODE score	Degree	Betweenness	Closeness
TNF	34.97	65.00	29.38	1.00
AKT1	34.97	65.00	29.38	1.00
IL6	34.97	65.00	29.38	1.00
VEGFA	34.97	65.00	29.38	1.00
ALB	34.97	65.00	29.38	1.00
JUN	34.97	65.00	29.38	1.00
PTGS2	34.97	64.00	26.87	0.98
TP53	34.97	64.00	27.35	0.98
MMP9	34.97	64.00	27.15	0.98
CASP3	34.97	64.00	26.55	0.98
EGF	34.97	63.00	25.13	0.97
IL1B	34.97	62.00	22.14	0.96
NFKBIA	36.03	62.00	23.80	0.96
HIF1A	34.97	62.00	23.13	0.96
CXCL8	33.18	61.00	20.72	0.94
FOS	36.03	61.00	21.89	0.94
FN1	34.54	60.00	20.59	0.93
CTNNB1	34.33	60.00	19.62	0.93
PPARG	33.99	60.00	21.76	0.93
IL10	34.82	59.00	17.02	0.92
MYC	36.26	59.00	18.22	0.92
EGFR	33.46	59.00	18.76	0.92
CCL2	35.05	58.00	16.48	0.90
MMP2	33.34	57.00	18.29	0.89
CCND1	35.03	56.00	15.98	0.88
IL2	34.74	55.00	13.74	0.87
ESR1	34.21	54.00	15.99	0.86
IL4	33.80	54.00	11.19	0.86
ICAM1	34.42	54.00	13.31	0.86
CD44	34.25	52.00	12.11	0.83
STAT1	34.67	52.00	10.84	0.83
HMOX1	32.67	52.00	11.50	0.83

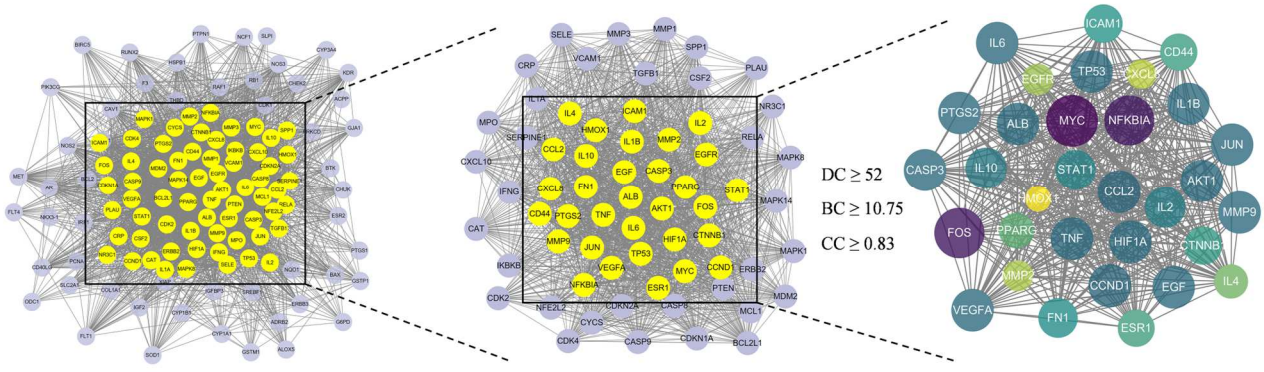

Fig. 3: Target interaction network diagram

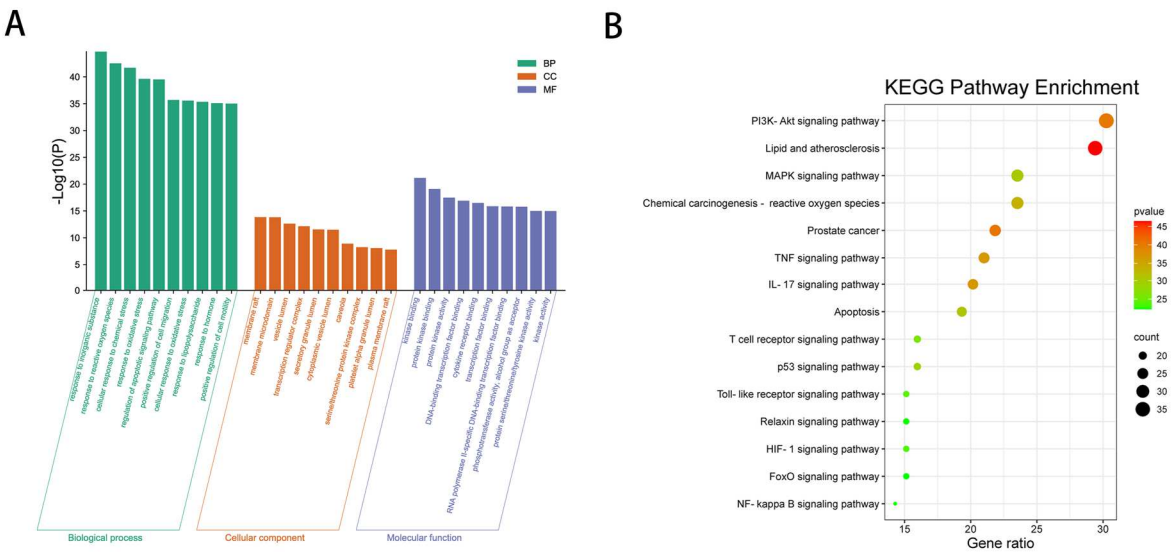

Fig. 4: GO and KEGG pathway enrichment analysis
(A) GO enrichment analysis; (B) KEGG enrichment analysis

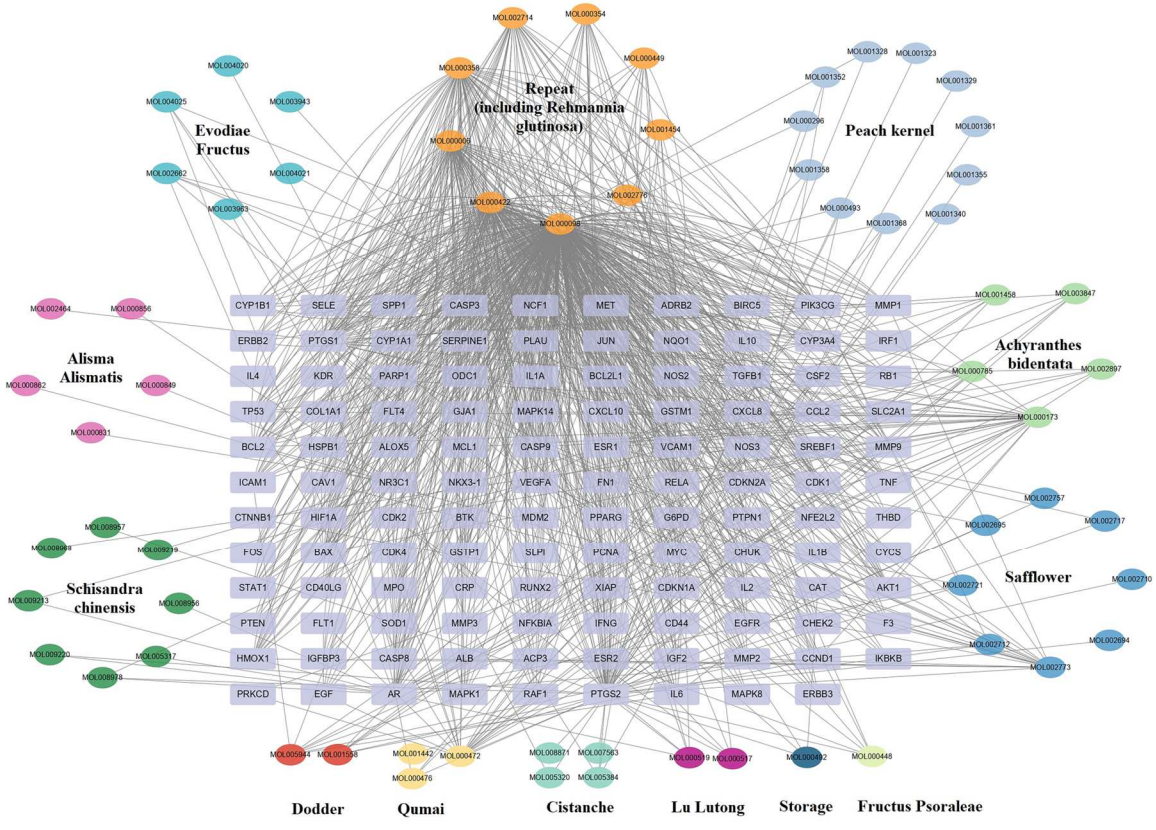

Fig. 5: Drug-active ingredient-target network diagram
The different colored bands in the outer ring represent the formula composition of QYTB, the circles of the same color in the outer ring represent the active ingredients of the Chinese medicine, the purple rectangle represents the target name, and the gray lines represent the interaction between the active ingredients and the targets.

Table 3: List of molecular docking affinities

Ligand	Affinity (kcal/mol)							
	AKT1	IL1B	IL6	TNF	MAPK1	CASP3	IL10	CXCL8
quercetin	-6.4	-7.2	-7.1	-6.9	-6.7	-7.7	-6.7	-8.2
kaempferol	-6.3	-7.0	-6.7	-6.9	-9.0	-7.6	-6.9	-7.9
beta-sitosterol	-6.4	-6.6	-5.8	-5.9	-7.1	-9.0	-8.6	-6.9
stigmasterol	-7.3	-7.0	-6.4	-7.2	-7.0	-8.1	-8.1	-7.3
luteolin	-6.4	-7.8	-7.2	-7.0	-9.1	-8.5	-6.9	-7.9

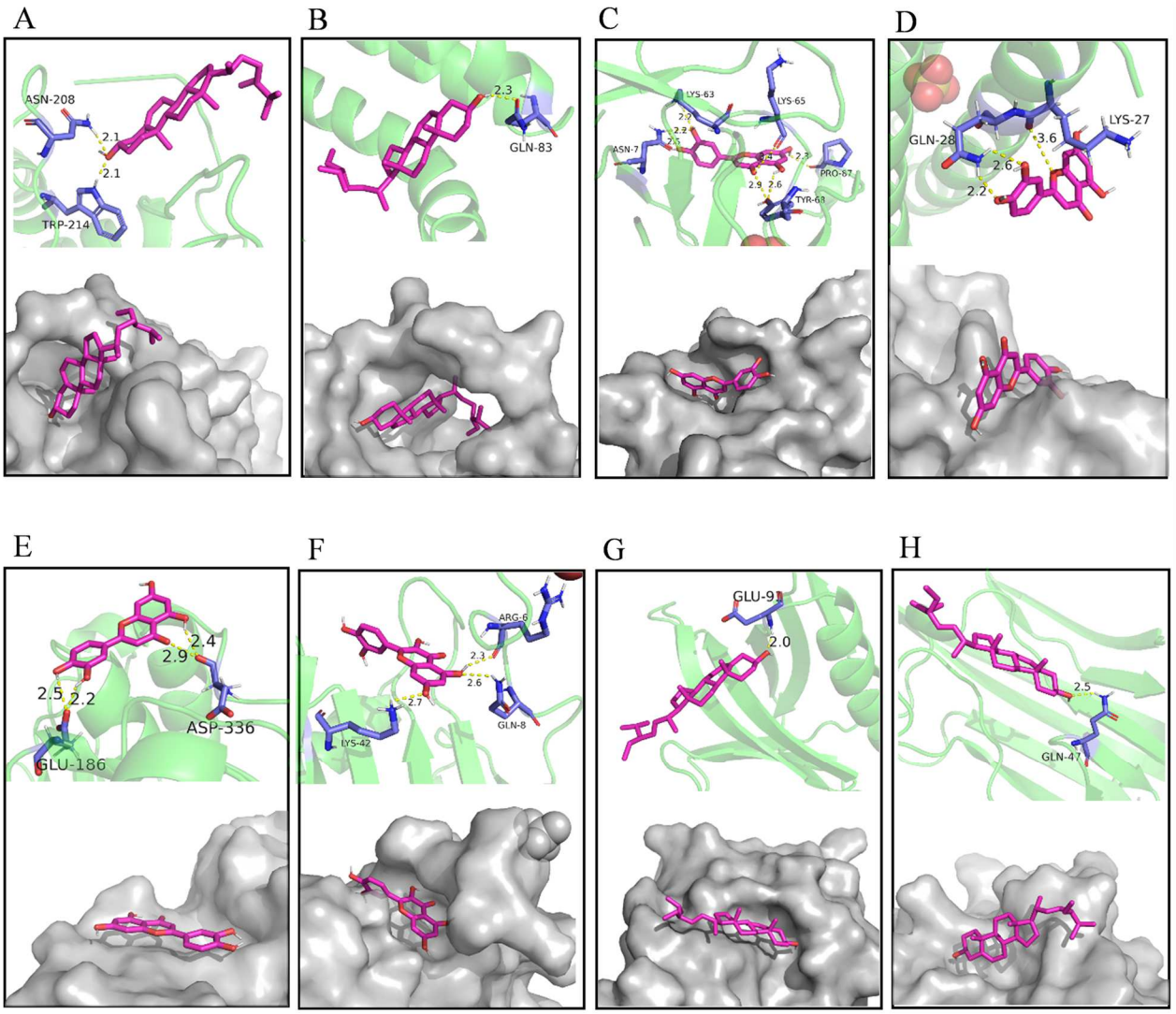

Fig. 6: Partial docking complex
(A) Beta-sitosterol and CASP3; (B) Beta-sitosterol and IL10; (C) Luteolin and IL1B; (D) Luteolin and IL6; (E) Luteolin and MAPK1; (F) Quercetin and CXCL8; (G) Stigmasterol and AKT1; (H) Stigmasterol and TNF.

The effect of QYTB on oxidative stress in SP-induced astrocytes

Consistent with the network pharmacology predictions suggesting that QYTB targets oxidative stress responses, the levels of superoxide dismutase (SOD), glutathione (GSH), catalase (CAT) and malondialdehyde (MDA) were measured using ELISA. Compared with the control group, the model group (SP-induced) exhibited significantly reduced concentrations of SOD, GSH and CAT ($P < 0.05$), coupled with a marked elevation in MDA levels ($P < 0.05$). Intervention with either QYTB-containing or levofloxacin-containing serum significantly reversed these trends, notably increasing SOD, GSH and CAT levels while decreasing MDA concentrations ($P < 0.05$).

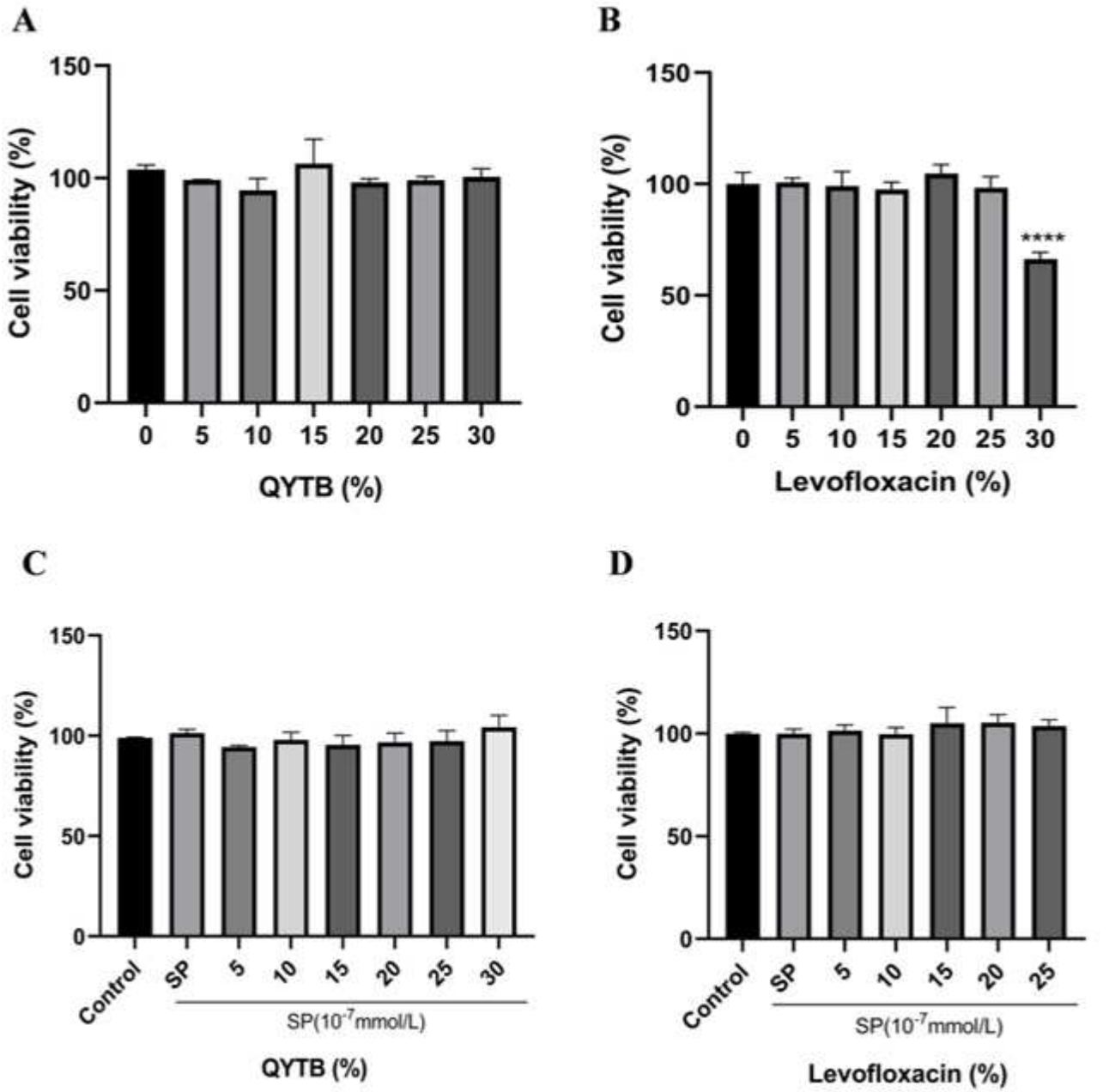

Fig. 7: Effect of serum containing different concentrations of QYTB and levofloxacin on the cell viability of SP-induced astrocytes compared with the group without levofloxacin
(A) QYTB; (B) Levofloxacin; (C) SP+QYTB; (D) SP+ Levofloxacin. **** $P < 0.0001$

Remarkably, the QYTB group demonstrated superior antioxidant capacity compared to the levofloxacin group, characterized by significantly higher levels of SOD, GSH and CAT and lower levels of MDA ($P < 0.05$) (Table 4, Fig. 9).

The effect of QYTB on core targets and MAPK signaling pathway in SP-induced astrocytes

Network pharmacology analysis identified TNF-α, IL-6 and IL-1β as primary core targets, with the MAPK signaling pathway emerging as the top-ranked pathway in KEGG enrichment. To validate these findings, the protein expressions of these inflammatory cytokines and key markers of the MAPK pathway were assessed via Western blot. The results revealed that both QYTB and levofloxacin significantly inhibited the expression of TNF-α, IL-6 and IL-1β, as well as the phosphorylation of p38MAPK and CREB in SP-induced astrocytes. Consistent with the antioxidant results, QYTB-containing serum exerted a more potent inhibitory effect on these protein expressions than the levofloxacin-containing serum (Fig. 9).

Table 4: SOD, GSH, MDA and CAT expression levels in different groups ($\bar{x}$±s, U/mgprot)

Group	SOD	GSH	MDA	CAT
Control	0.501±0.003	0.798±0.084	0.783±0.175	10.229±0.019
Model	0.367±0.013*	0.217±0.021*	16.862±1.277*	5.351±0.12#
Levofloxacin	0.424±0.013 Δ	0.288±0.021 Δ	10.597±0.914 Δ	7.637±0.275 Δ
QYTB	0.448±0.029 Δ #	0.375±0.103 Δ#	7.346±0.438Δ#	9.538±0.099 Δ #

*P<0.05, vs. Control; ΔP<0.05, vs. Model; #P<0.05, vs. Levofloxacin.

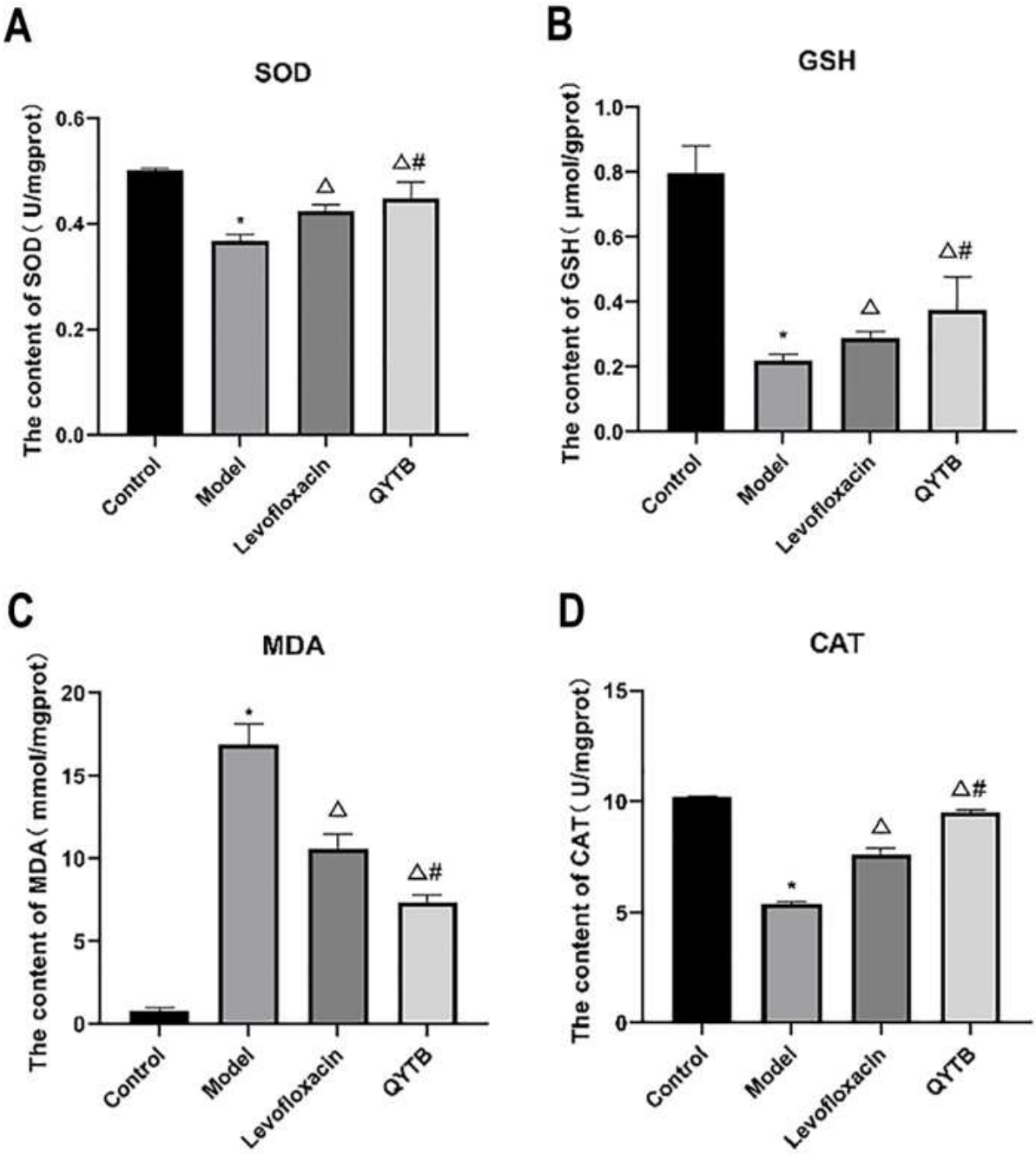

Fig. 8: Expression levels of SOD, GSH, MDA, and CAT in various cell groups.
(A) SOD; (B) GSH; (C) MDA; (D) CAT. *P<0.05, vs. Control; ΔP<0.05, vs. Model; #P<0.05, vs. Levofloxacin.

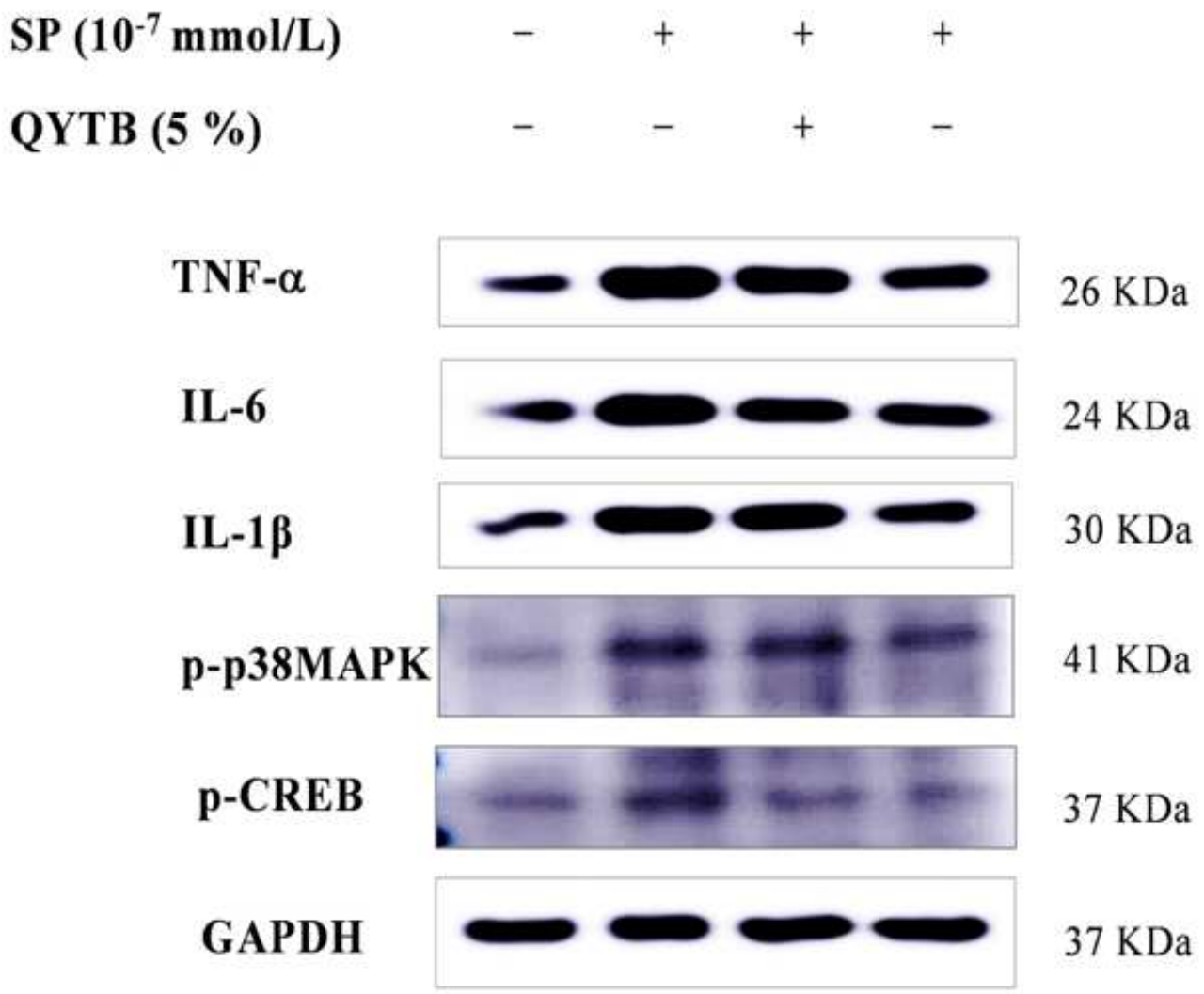

Fig. 9: Effects of QYTB and levofloxacin on SP-induced protein expression in spinal astrocytes

DISCUSSION

The pathogenesis of type III prostatitis is complex and multifactorial, involving an intricate interplay of inflammation, autoimmunity, oxidative stress, apoptosis and endocrine factors (Cheng *et al*., 2025). While acute inflammation typically serves as a protective response to microbial pathogens, its failure to resolve can trigger adaptive immunity, leading to a persistent chronic state characterized by extensive infiltration of lymphocytes and macrophages (Pena *et al*., 2021). Within this inflammatory milieu, macrophage-derived pro-inflammatory cytokines, such as TNF, IL-1β and IL-6, play a pivotal role in disease progression. Crucially, while these cytokines are associated with localized prostatic tissue damage, this study highlights their broader impact through the neuro-inflammatory component of chronic prostatitis/chronic pelvic pain syndrome (CP/CPPS). The systemic and paracrine release of these mediators in the spinal cord microenvironment—as modeled by the SP-induced astrocytes—reflects the central "cytokine storm" that perpetuates chronic pain signals. The observed reduction of TNF-α and IL-6 by QYTB in astrocytes suggest that the formula's clinical efficacy in relieving pelvic pain stems from its ability to suppress central neuroinflammation, moving beyond mere peripheral anti-inflammation.

Network pharmacology identified quercetin, kaempferol, β-sitosterol and luteolin as the primary active ingredients of QYTB, each possessing robust anti-inflammatory and antioxidant properties. Quercetin has been shown to improve pain sensitivity and prostate pathology by reducing pro-inflammatory mediators like IL-1β and TNF-α (Trivedi and Upadhyay, 2024). Kaempferol suppresses TNF-α release while promoting the secretion of the anti-inflammatory cytokine IL-10 (Dong *et al*., 2025). Furthermore, β-sitosterol impedes the activation of the NLRP3 inflammasome and the MAPK signaling pathway (Zheng *et al*., 2023), while luteolin inhibits T lymphocyte proliferation and decreases mediators like PGE2 (Xie *et al*.,

2021; Zhou *et al*., 2021). Collectively, these components enhance the activity of antioxidant enzymes such as SOD, GSH and CAT, contributing to the inhibition of oxidative stress. Consistent with network pharmacology predictions, *in-vitro* results confirmed that QYTB significantly inhibits core pro-inflammatory targets—TNF-α, IL-6 and IL-1β—which are pivotal drivers of prostatic inflammation and pain. In clinical settings, elevated levels of TNF-α in prostatic massage fluid are a hallmark of type III prostatitis (Zhang *et al*., 2025) and TNF antagonists have been shown to alleviate epithelial hyperplasia and macrophage-mediated inflammatory responses (Vickman *et al*., 2022). Similarly, the upregulation of IL-6 is involved in the regulation of autophagy and is closely linked to the NLRP3 inflammasome in prostatitis models (Chen *et al*., 2021). By suppressing these cytokines, QYTB effectively disrupts the self-perpetuating cycle of inflammation and pain.

Oxidative stress further exacerbates the development of type III prostatitis by inducing tissue injury and fibrosis (Song *et al*., 2023). Excessive reactive oxygen species (ROS) production under pathological conditions leads to decreased antioxidant activity and the accumulation of oxidative products like MDA, causing inflammatory tissue damage (Li *et al*., 2021). Because oxidative stress is known to increase neuronal excitability, the restoration of redox homeostasis by QYTB in astrocyte model implies a protective effect against oxidative-induced neurotoxicity. In a clinical context, this translates to a reduction in the pathological remodeling of pain pathways within the spinal dorsal horn. This research demonstrates that serum enriched with QYTB markedly elevates SOD, GSH and CAT levels while significantly reducing MDA concentrations in SP-induced astrocytes, thereby alleviating cellular damage through multi-target regulation (Li *et al*., 2021; Wan *et al*., 2024).

Finally, the authors identified the p38MAPK/CREB pathway as a critical driver of central sensitization. In clinical type III prostatitis, persistent noxious stimuli from the prostate sustain the phosphorylation of these proteins in spinal glia, effectively lowering the pain threshold. The p38MAPK family mediates cellular responses to cytokines and stressors, acting as a key regulator in the biosynthesis of pro-inflammatory cytokines (Galganska *et al*., 2023). The findings demonstrate that QYTB inhibits the p38 MAPK/CREB axis in spinal astrocytes more effectively than the positive control, levofloxacin. This provides a molecular link between the formula's pharmacological action and the clinical attenuation of referred pain and voiding dysfunction (Liu *et al*., 2023). In summary, QYTB enhances therapeutic outcomes for type III prostatitis by diminishing the expression of pro-inflammatory mediators and impeding the overactivation of the MAPK signaling cascade.

CONCLUSION

In conclusion, this study demonstrates that QYTB effectively enhances the concentration of antioxidant enzymes (SOD, CAT and GSH) while significantly reducing the levels of malondialdehyde (MDA) in SP-induced spinal astrocytes. Furthermore, QYTB notably downregulates the expression of key pro-inflammatory cytokines, including IL-1β, TNF-α and IL-6 and inhibits the phosphorylation of p38MAPK and CREB proteins within the MAPK signaling pathway. These results suggest that QYTB exerts potent anti-inflammatory and antioxidant effects, providing a robust scientific basis for its therapeutic application in the management of type III prostatitis through the modulation of neuroinflammatory and oxidative stress pathways.

Acknowledgements
We would like to thank the National Natural Science Foundation of China for their funding support. We also appreciate Henan University of Chinese Medicine for providing the experimental facilities and venue.

Author's contributions
Miaomiao Ma: Conceptualization, Data curation, Formal analysis, Investigation, Methodology, Software and Writing – original draft, Writing – review and editing; Zulong Wang: Conceptualization, Funding acquisition, Project administration, Supervision, Validation and Writing – review and editing; Baojun Ju: Funding acquisition, Resources, Visualization, Writing – original draft and Writing – review and editing.

Funding
This research is financially supported by the Henan Provincial Traditional Chinese Medicine Key Discipline (TCM Surgery) Construction Project.

Data availability statement
The datasets generated and/or analysed during the current study are available from the corresponding author on reasonable request.

Ethical approval
The experimental procedures were approved by the Animal Ethics Committee of the Henan Academy of Chinese Medicine, (Ethics No. 202307033) and were conducted in compliance with the ARRIVE guidelines. This study was performed in adherence with the ARRIVE guidelines. See supplementary file for the ARRIVE checklist.

Conflict of interest
The authors declare that they have no known competing financial interests or personal relationships that could have appeared to influence the work reported in this paper. The authors declare no conflict of interest.

Supplementary data

https://www.pjps.pk/uploads/2026/07/SUP1785064541.pdf

REFERENCES

Borgert BJ, Wallen EM and Pham MN (2025). Prostatitis: A review. *JAMA*, **334**(11): 1003-1013.

Chen L, Wang H, Ge S and Tai S (2021). IL-6/STAT3 pathway is involved in the regulation of autophagy in chronic non-bacterial prostatitis cells and may be affected by the NLRP3 inflammasome. *Ultrastruct. Pathol.*, **45**(4–5): 297–306.

Cheng T, Ning J, Ye D, Zha Z, Xu W, Fang W, Mao L and Gu M (2025). Analysis of the positive influence of Qianlie Shutong capsule combined with tamsulosin on prostate health of patients with prostatitis. *Pak J Pharm Sci*, **38**(4):1328-1333.

Dong H, Song G, Wang Z, Wu X, Wang Q and Wang YH (2025). Kaempferol as a multifaceted immunomodulator: Implications for inflammation, autoimmunity and cancer. *Front Immunol*, **16**: 1671519.

Gałganska H, Jarmuszkiewicz W and Galganski L (2023). Carbon dioxide and MAPK signalling: Towards therapy for inflammation. *Cell Commun Signal*, **21**(1): 280.

Ge L, Ma L, Jin Z (2025). Investigating the impact of aspartame on ulcerative colitis through network toxicology and molecular docking. *Food Sci Nutr,* **13**(9): e70869.

Jiang Z, Luo W, Liu L and Long Z (2024). Enhancement sensitivity of TRPV1 in dorsal root ganglia via the SP-NK-1 pathway contributes to increased bladder organ sensitivity caused by prostatitis. *Front Neurosci*, **18**: 1484980.

Li S, Li Y, Su X, Han A, Cui Y, Lv S, Zhang J and Li C (2021). Dihydroartemisinin promoted bone marrow mesenchymal stem cell homing and suppressed inflammation and oxidative stress against prostate injury in chronic bacterial prostatitis mice model. *Evid-Based Compl Alt*, **2021**: 1829736.

Liu Q, Zhang X, Mao P, Wang Z, Mao Q, Wang C, Liu J, Zhu X, Wang B and Wei H (2023). Shuangshi Tonglin capsule improves chronic prostatitis through the SIRT-1/AMPK and MAPK signalling pathways. *Heliyon*, **9**(11): e21745.

Ma X, Lao Y, Bai Y, Guan X, Jiang J, Cui M, Dong Z (2025). Study progress of etiologic mechanisms of chronic prostatitis/chronic pelvic pain syndrome. *Int Immunopharmacol.,* **148**: 114128.

Nürnberger F, Rummel C, Ott D, Gerstberger R, Schmidt MJ, Roth J and Leisengang S (2023). Gabapentinoids suppress lipopolysaccharide-induced interleukin-6 production in primary cell cultures of the rat spinal dorsal horn. *Neuroimmunomodulation*, **30**(1): 1-14.

Pena VN, Engel N, Gabrielson AT, Rabinowitz MJ and Herati AS (2021). Diagnostic and management strategies for patients with chronic prostatitis and chronic pelvic pain syndrome. *Drug Aging*, **38**(10): 845–886.

Qin Z, Zhang C, Guo J, Kwong JSW, Li X, Pang R, Doiron RC, Nickel JC and Wu J (2022). Oral pharmacological treatments for chronic prostatitis/chronic pelvic pain syndrome: A systematic review and network meta-analysis of randomised controlled trials. *Eclinicalmedicine*, **48**: 101457.

Song W, Gao J, Huang J, Liu Y, Long Z and He L (2023). Is type III prostatitis also associated with bacterial infection?. *Front Cell Infect Mi*, **13**: 1189081.

Trivedi R and Upadhyay TK (2024). Preparation, characterization and antioxidant and anticancerous potential of quercetin loaded β-glucan particles derived from mushroom and yeast. *Sci Rep-Uk*, **14**(1): 16047.

Valipour R, Narouie B, Rastgou A, Dadpour M, Radpour N, Momeni H, Momeni A, Ahmadzade M, Rouientan H, Jadidi S and Saygin S (2025). Evaluation of concomitant treatment for chronic pelvic pain syndrome. *Urologia*, **92**(3): 525-528.

Vickman RE, Aaron-Brooks L, Zhang R, Lanman NA, Lapin B, Gil V, Greenberg M, Sasaki T, Cresswell GM, Broman MM, Paez JS, Petkewicz J, Talaty P, Helfand BT, Glaser AP, Wang CH, Franco OE, Ratliff TL, Nastiuk KL, Crawford SE and Hayward SW (2022). TNF is a potential therapeutic target to suppress prostatic inflammation and hyperplasia in autoimmune disease. *Nat Commun*, **13**(1): 2133.

Wan R, Su Y, Zhu M and Huang Y (2024). Elevated blood malondialdehyde level contributed to a high stroke risk in a Chinese elderly population from rural areas: A cross-sectional study. *Sci Rep-Uk*, **14**(1): 4325.

Xie K, Chai Y, Lin S, Xu F and Wang C (2021). Luteolin regulates the differentiation of regulatory T cells and activates IL-10-dependent macrophage polarization against acute lung injury. *J Immunol Res*, **2021**: 1–12.

Zbiciak-Nylec MA, Brzezinska-Wcislo L, Salwowska N (2021). The efficacy of antimalarial drugs in the therapy of selected forms of cicatricial alopecia. *Postepy Dermatol Alergol*, **38**(2): 302-309.

Zhang XM, Li WY, Hao ZY, Zhou L, Yang C, Du HX and Liang CZ (2025). The “prostate-pelvic syndrome” theory used in patients with type-III prostatitis and its correlation with prostate volume. *BMC UROL*, **25**(1): 9.

Zheng Y, Zhao J, Chang S, Zhuang Z, Waimei S, Li X, Chen Z, Jing B, Zhang D and Zhao G (2023). β-sitosterol alleviates neuropathic pain by affect microglia polarization through inhibiting TLR4/NF-κB signaling pathway. *J Neuroimmune Pharm*, **18**(4): 690–703.

Zhou W, Hu M, Hu J, Du Z, Su Q and Xiang Z (2021). Luteolin suppresses microglia neuroinflammatory responses and relieves inflammation-induced cognitive impairments. *Neurotox Res*, **39**(6): 1800–1811.